PHYSICAL REVIEW B **99**, 134520 (2019)

# Surface terminations and layer-resolved tunneling spectroscopy of the 122 iron pnictide superconductors

Ang Li,[1,*] Jia-Xin Yin,[2] Jihui Wang,[1] Zheng Wu,[1] Jihua Ma,[1,3] Athena S. Sefat,[4] Brian C. Sales,[4] David G. Mandrus,[4] Michael A. McGuire,[4] Rongying Jin,[5] Chenglin Zhang,[6] Pengcheng Dai,[6] Bing Lv,[1,†] Ching-Wu Chu,[1] Xuejin Liang,[2] P.-H. Hor,[1] C.-S. Ting,[1] and Shuheng H. Pan[1,2,7,8,9,‡]

[1]*Department of Physics and Texas Center for Superconductivity, University of Houston, Houston, Texas 77204, USA*
[2]*Beijing National Laboratory for Condensed Matter Physics and Institute of Physics, Chinese Academy of Sciences, Beijing 100190, China*
[3]*Department of Physics, Boston College, Chestnut Hill, Massachusetts 02467, USA*
[4]*Materials Science & Technology Division, Oak Ridge National Laboratory, Oak Ridge, Tennessee 37831, USA*
[5]*Department of Physics & Astronomy, Louisiana State University, Baton Rouge, Louisiana 70803, USA*
[6]*Department of Physics and Astronomy, Rice University, Houston, Texas 77005, USA*
[7]*School of Physics, University of Chinese Academy of Sciences, Beijing 100190, China*
[8]*CAS Center for Excellence in Topological Quantum Computation, University of Chinese Academy of Sciences, Beijing 100190, China*
[9]*Songshang Lake Material Laboratory, Dongguan, Guangdong 523808, China*

(Received 25 April 2017; revised manuscript received 28 March 2019; published 30 April 2019)

The surface terminations of 122-type alkaline earth metal iron pnictides $AE\mathrm{Fe_2As_2}$ ($AE$ = Ca, Ba) are investigated with scanning tunneling microscopy/spectroscopy. Cleaving these crystals at a cryogenic temperature yields a large majority of terminations with an atomically resolved $(\sqrt{2}\times\sqrt{2})$R45 or $1\times2$ lattice, as well as a very rare termination of $1\times1$ lattice symmetry. By analyzing the lattice registration and selective chemical marking, we identify these terminations as $(\sqrt{2}\times\sqrt{2})$R45-reconstructed *AE*, $1\times2$-reconstructed As, and $(\sqrt{2}\times\sqrt{2})$R45-reconstructed Fe surface layers, respectively. Layer-resolved tunneling spectroscopy on these terminating surfaces reveals a well-defined superconducting energy gap on the As terminations, while the gap features become weaker on the *AE* terminations and absent on the Fe terminations. The superconducting gap is hardly affected locally by the As or *AE* surface reconstructions. The definitive identification of the surface terminations and the associated spectroscopic signatures shed light on the essential roles of As and the pnictogen-iron-pnictogen trilayer building block in iron-based superconductivity.

DOI: 10.1103/PhysRevB.99.134520

## I. INTRODUCTION

The discovery of iron-based superconductors marked significant progress in the study of high-temperature superconductivity [1–3]. All iron-based superconductors share a unique pnictogen (chalcogen)-iron-pnictogen (chalcogen) trilayer structural unit, and it is generally believed that superconductivity develops primarily in the iron plane with *3d* orbital characters [4]. To unravel the multiorbital nature of the iron plane and to understand the roles of other ingredient layers, an atomic layer-resolved electronic characterization is thus essential. Scanning tunneling microscopy/spectroscopy (STM/STS) is an ideal tool for extracting local structural and spectroscopic information. It has played a critical role in exploring the electronic interactions in iron-based superconductors [5]. So far, iron-based superconductors like Fe(Se,Te) and LiFeAs have been relatively well characterized by STM/STS due to their definitive crystal cleavage, while the study of 122-type alkaline earth metal iron pnictides $AE\mathrm{Fe_2As_2}$ ($AE$ = Ca, Ba, etc.) suffers from controversial identifications of the cleavage planes due to the complex surface morphologies [6–23]. Therefore, clarification of the cleavage, identification of the resulting terminations, and subsequent layer-resolved spectroscopic investigations become crucial and highly demanded for studying the *AE*122 iron-based superconductivity.

Among iron-based superconductors, the *AE*122 compounds are noteworthy for their relatively high $T_C$ and widely accessible chemical doping range [2,3]. They have a layered crystal structure with the weakest bonding between the adjacent *AE* and As layers [Fig. 1(a)]. Accordingly, these crystals tend to cleave there between and the *AE* and As planes are most likely to be exposed as the surface terminations. As the adjacent As layer and *AE* layer are ionically bonded in bulk, upon cleaving, the unbalanced charge distribution on the terminations can lead to various surface reconstructions making the surface identification more complicated. Based on the early STM studies [6–23], two major assignments have been proposed for the *AE*122-crystal surface terminations: (1) Upon cleaving, the *AE* atoms are divided statically into two 50% portions that redistribute uniformly onto the two adjacent As terminating surfaces to form either a $(\sqrt{2}\times\sqrt{2})$R45 or a $1\times2$ superstructure as a 50%

---

[*] Corresponding author: angli@mail.sim.ac.cn; current address: State Key Laboratory of Functional Materials for Informatics, Shanghai Institute of Microsystem and Information Technology, Chinese Academy of Sciences, Shanghai 200050, China.

[†] Current address: Department of Physics, The University of Texas at Dallas, Richardson, Texas 75080, USA.

[‡] Corresponding author: span@iphy.ac.cn

2469-9950/2019/99(13)/134520(6)

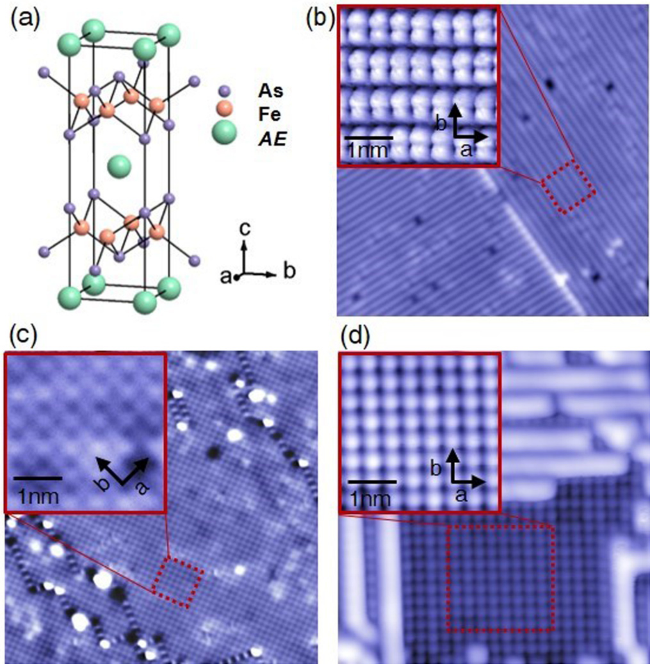

FIG. 1. (a) Schematic crystal structure of $AE\mathrm{Fe_2As_2}$. (b)–(d) Surface morphologies demonstrating (b) $1 \times 2$ (V = 100 mV, I = 30 pA), (c) rt2 (V = 20 mV, I = 0.2 nA), and (d) $1 \times 1$ (V = 50 mV, I = 2 nA) superstructures. Insets in (b)–(d) are the zoom-in image of $1 \times 2$ dimers (V = 20 mV, I = 8 nA), rt2 buckling (V = 20 mV, I = 2 nA) and $1 \times 1$ surface (V = 50 mV, $I$ = 2 nA), respectively.

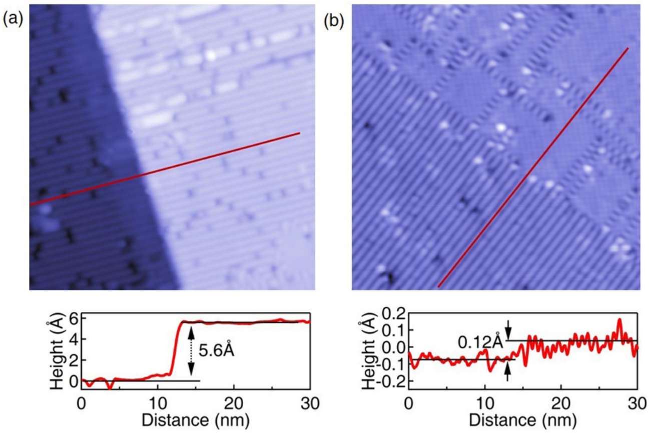

FIG. 2. (a) The step height of ~5.6 Å between two stripe surfaces, which is consistent with the crystallographic dimension of a half unit cell $c/2 = 5.8$ Å. (b) The step between a rt2 surface and a stripe surface with the apparent step height of ~0.12 Å, which is one order of magnitude too small than any of the crystallographic spacing in this crystal. For both cases, the topological profile along the line marked in the upper topographic image is shown in the lower panel. Data are both taken on $\mathrm{CaFe_2As_2}$ at 4.2 K for an area of $300\times300$ Å$^2$ with tunneling junction set up: V = 50 mV, I = 0.5 nA.

*AE* coverage [6–9,12,14,19–23]; (2) the *AE* atomic layer is disassembled into scattered atoms, clusters, or lumps instead of remaining in a complete atomic coverage layer, then the As layer is exposed with $(\sqrt{2} \times \sqrt{2})$R45 or $1 \times 2$ reconstruction [10,11,13,18]. In this article we present high-resolution STM/STS results on the cryogenically cleaved $AE\mathrm{Fe_2As_2}$ [$\mathrm{Ba(Fe_{1-x}Co_x)_2As_2}$, $\mathrm{Ba_{1-x}K_xFe_2As_2}$, and $\mathrm{CaFe_2As_2}$] single crystals. We demonstrate that three types of ordered surface structure can be distinguished as (1) $(\sqrt{2} \times \sqrt{2})$R45 reconstruction of the complete *AE* lattice, (2) $1 \times 2$ stripes from the As dimerization, and (3) the rarely observed $(\sqrt{2} \times \sqrt{2})$R45 pattern of the Fe lattice. Local differential conductance measurements show superconducting gap features in the low-energy excitation spectra on both *AE* and As terminations, while not in that on the Fe exposure. Such spectroscopic discrepancies indicate that the As-Fe-As trilayer structure is essential to the superconducting pairing in iron pnictides.

## II. EXPERIMENTAL METHOD

The single crystalline samples of $\mathrm{BaFe_2As_2}$ and $\mathrm{CaFe_2As_2}$ with various doping were grown using the self-flux method [24–26]. In particular, the $\mathrm{CaFe_2As_2}$ crystals were furnace-cooled to room temperature without quenching, thus no trace of a low-temperature collapsed tetragonal phase was detected in the electrical resistivity and magnetic susceptibility measurements [27]. The STM/STS experiments were carried out on a home-built ultrahigh vacuum low-temperature STM. Samples were cleaved *in situ* below 30 K and immediately transferred to the STM head, which was already at the base temperature of 4.3 K. The scan tips were prepared from polycrystalline tungsten wires by electrochemical etching and subsequent field-emission cleaning. Topographic images were acquired in the constant-current mode with the bias voltage applied to the sample. Differential conductance spectra were recorded with the standard lock-in technique. When describing the lattice symmetry, we choose the $\mathrm{ThCr_2Si_2}$-type tetragonal notation throughout this article so that the low-temperature orthorhombic symmetry [28] can be denoted as "$(\sqrt{2} \times \sqrt{2})$R45", or "rt2" for short.

## III. RESULTS AND DISCUSSION

The most commonly (about 99% of the time) observed terminating surfaces of an $AE\mathrm{Fe_2As_2}$ single crystal resulted from cold cleaving are shown in Figs. 1(b) and 1(c). The $1 \times 2$ superstructure in Fig. 1(b) consists of one-dimensional stripes with interstripe distance ~8 Å, twice the tetragonal lattice constant. Along the stripe are grains at ~4 Å spacing and within each grain there are two atoms that can be resolved to form a dimer in high-resolution images [inset in Fig. 1(b)]. This dimerization can follow either the *a* or *b* direction, thus twin domain structures are often observed on a striped surface as shown in Fig. 1(b). The dimerization is most likely a surface phenomenon for no evidence has been reported from bulk measurements such as x-ray diffraction and high-resolution transmission electron microscope. The structural nature of the $1 \times 2$ symmetry is further evidenced by the independence of topographic image on the bias voltage. The second type of termination shown in Fig. 1(c) exhibits a bias-independent square-like lattice with a much smaller topographic corrugation. There, the unit cell is enlarged by $\sqrt{2} \times \sqrt{2}$ times from the tetragonal $1 \times 1$ base and it seems that only 50% of the atoms in the atomic layer are resolved if one attempts to assign them to the *AE* or As layer. High-resolution imaging, however,

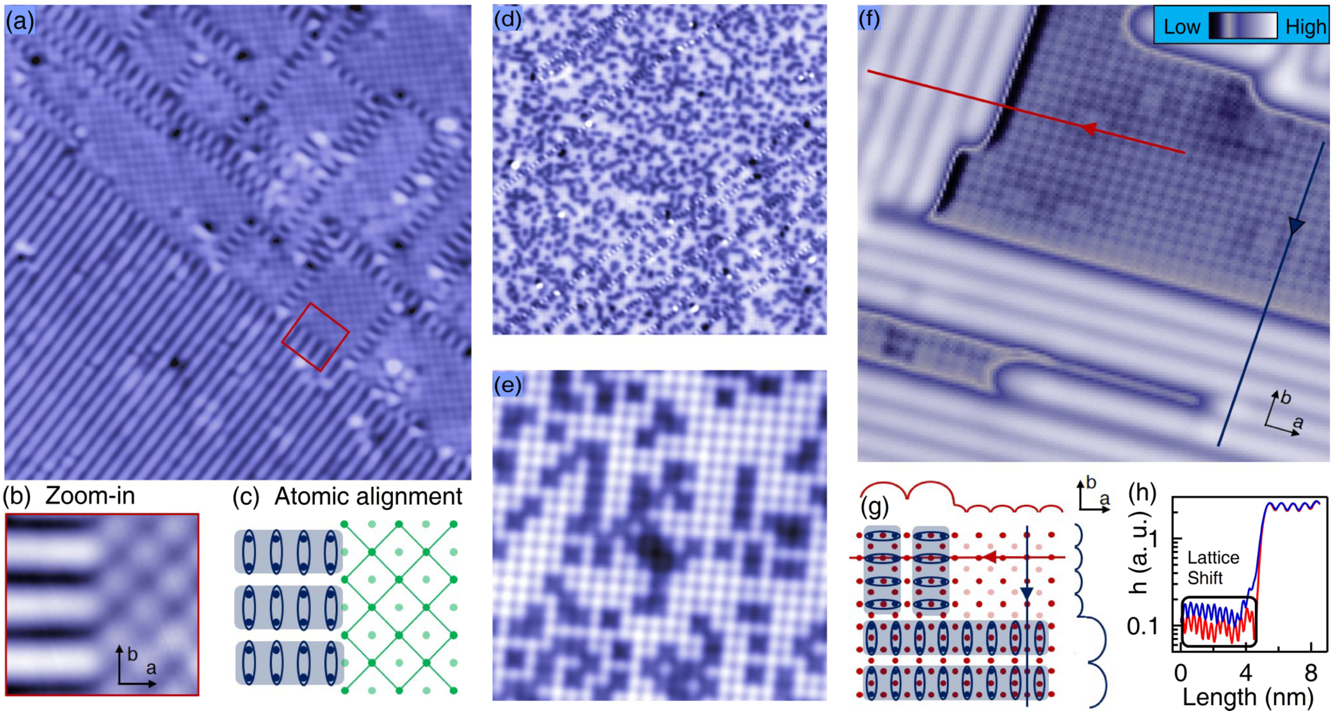

FIG. 3. (a) The joint area between rt2 and 1 × 2 in $CaFe_2As_2$ ($400\times400$ Å$^2$, V = 50 mV, I = 1 nA). (b) The zoom-in images of boundaries as marked in the red box in (a). (c) Schematic drawings for the in-plane atomic lattice registration at joint boundary of 1 × 2 and rt2 areas when they belong to two different atomic layers (As and *AE*). Ellipses and solid lines represent the dimers and rt2 superlattice respectively. The rt2 topographies of $Ba_{0.6}K_{0.4}Fe_2As_2$ are shown in (d) $500\times500$ Å$^2$, V = −100 mV, I = 2 nA, and (e) $125\times125$ Å$^2$, V = 100 mV, I = 2 nA. (f) 1 × 1 area surrounded by the 1 × 2 stripes in $CaFe_2As_2$ ($130\times130$ Å$^2$, V = 50 mV, I = 1 nA). (g) Schematic drawings for the in-plane atomic arrangement of stripes vs 1 × 1 lattice assuming that 1 × 1 is rt2-buckled Fe (As: dark blue, Fe: dark and light red), and the height profiles along the two orthogonal directions. (h) Height profiles along the 1 × 1 lattice in orthogonal directions indicated in (f). A half-unit-cell lattice shift in the 1 × 1 profile relative to the stripe profile can be clearly observed.

reveals the complete atomic coverage with a $\sqrt{2}\times\sqrt{2}$ buckling reconstruction [inset in Fig. 1(c)]. Such a rt2 lattice reconstruction is consistently observed even in heavily overdoped $Ba(Fe_{1-x}Co_x)_2As_2$ samples, where the bulk low-temperature orthorhombic/magnetic phase is completely suppressed [29]. Therefore, we conclude that the buckled rt2 superstructure is a surface phenomenon as well. In addition to 1 × 2 and rt2, a third type of surface morphology with 1 × 1 lattice symmetry [Fig. 1(d)] is very rarely observed. Knowing the easy cleavage plane lies between the *AE* and As layers, we expect the commonly observed 1 × 2 and rt2 surfaces are associated with the *AE* and/or As terminations exposed after cold cleaving.

As the *AE* and As layers share the same crystal lattice symmetry in the bulk, it is not decisive to assign the atomic identity of the 1 × 2 or rt2 reconstructed surface merely based on the structural symmetry. Due to the fact that the constant current topographic image convolutes the spatial variation of the integrated local density of states (LDOS) and the geometrical corrugations, simply assigning these terminations by their apparent image height would not be appropriate either. As an example, on a cleaved $CaFe_2As_2$ crystal, while the apparent step height between two stripe surfaces is consistent with the crystallographic dimension of a half unit cell $c/2$ [Fig. 2(a)], the apparent step height between a rt2 surface and a stripe surface in its STM image is one order of magnitude too small than any of the crystallographic spacings in the bulk crystal [Fig. 2(b)]. This clearly demonstrates that it is impossible to rely on the apparent step height in determination of the identities of two surfaces with different chemical identities or superstructures, not even to determine whether they are two different elemental terminations or simply the same elemental termination but with different surface reconstructions.

After carefully examining these topographic images and comparing with the crystal structures, we have developed a set of practical schemes to help in identifying these terminations. First, we apply the relative lattice registration scheme and have noticed a critical clue from the in-plane lattice alignment between the adjacent 1 × 2 and rt2 regions in Fig. 3(a). The zoom-in image shown in Fig. 3(b) clearly demonstrates that the centerline of each stripe points in 45°exactly to the rt2 superlattice grid, indicating the two atomic lattices' half-unit-cell alignment. This observation supports the fact that the two commonly observed surface structures are not from the same atomic plane, but are associated with *AE* and As terminations, respectively, as shown in the schematic in Fig. 3(c). Second, we apply the selective doping scheme to determine their correspondence. As an example, we chose potassium to dope $BaFe_2As_2$, in which potassium dopants partially substitute the Ba atoms [20]. In its rt2 topographic images [Fig. 3(d) and 3(e)], bright and dark sites are readily visible at atomic level, while such a contrast is absent in the 1 × 2 stripes. The percentage of dark sites is approximately 40%, and agrees fairly well with the nominal concentration of K doping. This leads us to conclude that the two major surface terminations are created by cold cleaving between *AE* and As planes; the exposed *AE* layer buckles to form a rt2-superstructure and the As atoms in the arsenic plane dimerize to form one-dimensional stripes. Each of the two terminations alone does not cover the entire cleaving surface. Instead, the entire surface is covered by a roughly 50–50% mixture of them that are separated by single-atom steps [Fig. 2(b)]. The apparent step height of such single-atom step in the STM topographic images is much smaller (∼0.7 Å for $BaFe_2As_2$ and ∼0.1 Å for $CaFe_2As_2$) as compared to the crystalline *AE*-As interlayer distance (1.9 Å [28]), which can be explained by *AE*'s smaller contribution to the density of states near the Fermi level [30].

Having identified the commonly observed rt2 and 1 × 2 terminations, we then turn to the rare 1 × 1 termination [Figs. 1(d) and 3(f)]. Considering its very low probability of occurrence, the 1 × 1 termination could be either an unreconstructed version of the *AE* or As exposure [22,31] or the $(\sqrt{2}\times\sqrt{2})R45$ reconstructed pattern of the Fe lattice (whose original lattice constant is $1/\sqrt{2}$ times of that in As and *AE*). Again, we apply the lattice registration scheme. Note that the rt2 pattern of Fe, when surrounded by As stripes, should have a unique atomic registration with the As stripes from two orthogonal directions as illustrated in Fig. 3(g). There is a half-unit-cell shift in the alignment of rt2 Fe lattice with respect to the As stripes from the *a* and *b* directions. We emphasize that this atomic lattice registration is exclusive for Fe terminations with rt2 reconstruction. The height profiles along the two lines in Fig. 3(f) clearly demonstrate such a lattice registration with a half-unit-cell shift as highlighted in Fig. 3(h), which provides decisive evidence of the 1 × 1 structure being the rt2 reconstructed pattern of the unusually exposed Fe layer.

The combination of low temperature cleaving and the definitive identification of all building layers provide one an extraordinary opportunity to perform layer-resolved spectroscopic investigations of $AEFe_2As_2$. In Fig. 4, the spatially averaged differential conductance spectra on optimally doped $Ba(Fe,Co)_2As_2$ ($T_C \approx 22$ K) show the superconducting energy gap on both Ba and As terminations with the gap magnitude $\Delta \approx 6$ meV and the ratio $2\Delta/k_BT_C \approx 6.3$, indicating a strong coupling superconducting state. Interestingly, the gap features are well defined in the 1 × 2 As surface, while the spectrum on Ba termination exhibits reduced coherence peaks and more in-gap states near the Fermi level, probably caused by impurity scattering effect of Co doping. The more general discussion of the spectral differences from these two terminations is still open, and we present our view from the orbital perspective [32].

In strong contrast, the Fe termination is characterized by an overall V-shaped spectrum without features of superconductivity. This is quite puzzling as that even if there is no coherent Cooper pairing in the exposed Fe layer due to the missing As coverage, there should still be a superconducting gap feature from the proximity of superconducting bulk lying below. A possible scenario is that a metallic state coexists in the region (caused by the surface termination/reconstruction) and obscures the observation of the proximity induced superconducting gap. If this is the case, then why this metallic state is immune to the proximity effect needs an explanation. A possibility along another line is that magnetism can suppress the phase coherence of Cooper pairs [33], thus it is conceivable that without coverage of As, the Fe-terminated surface possesses strong magnetism that destroys the superconducting phase coherence. If this is the case, one should still see a gap-like DOS depression without coherent peaks in the tunneling spectrum, but this feature is absent. In any case, the V-shaped spectrum without any superconducting gap features on the exposed Fe surface compared with the coherent gap spectrum on the As surface essentially highlights the role of the As layer and the vital integrity of the As-Fe-As trilayered block in the electronic pairing and the emergence of superconductivity. Indeed, the magnetic and electronic properties depend very sensitively on the Fe-As local structures [34,35]. Removing the As layer can dramatically alter the coordination environment of Fe, hence the pairing of electrons.

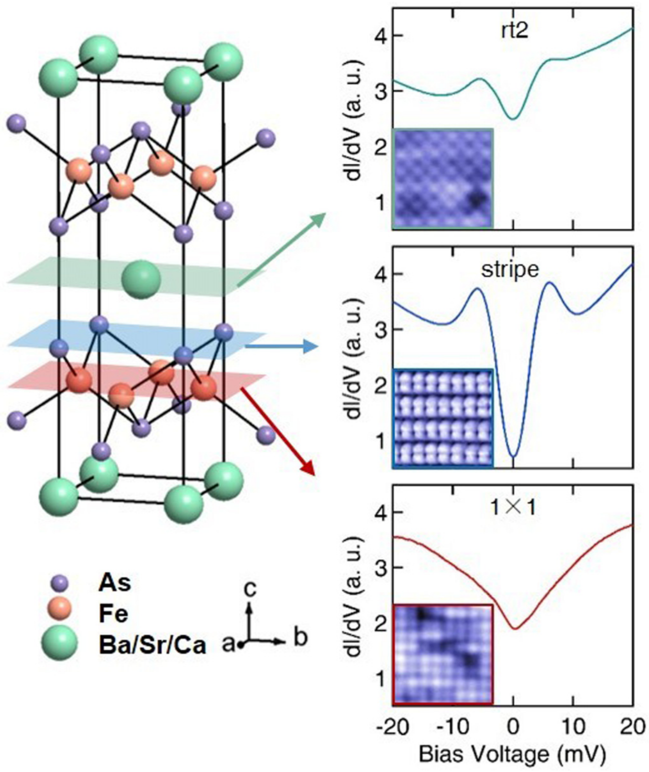

FIG. 4. Spatially averaged differential conductance spectra on three surface terminations in optimally doped $Ba(Fe,Co)_2As_2$ ($V = -20$ mV, $I = 0.67$ nA). The insets show the corresponding topographic images with the size of $35\times35$ Å$^2$.

In addition to the chemical identity, the lattice reconstruction can also influence the surface electronic structure by inducing band folding in the momentum space. Our previous photoemission measurement shows that the 1 × 2 surface reconstruction leads to a noticeable band folding, with the band around the Γ and M point of the Brillion zone being folded to the X position [36]. In our STM/S observations, the representative broken symmetry in the *AE* and As terminations, however, does not alter the low-energy local DOS spectrum significantly. For example, no perceivable change in the gap size is detected with 1 × 2 periodicity [Figs. 5(a) and 5(b)],

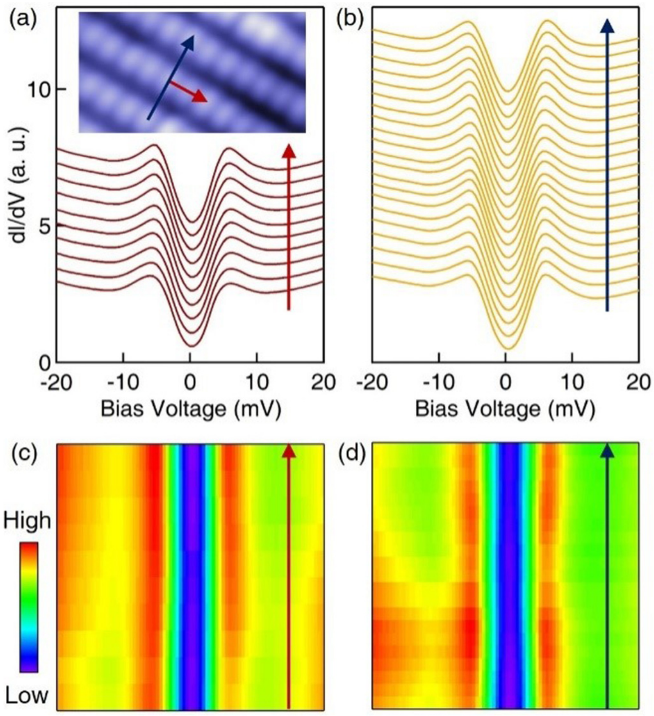

FIG. 5. (a) and (b) Series of differential conductance spectra measured along and across the As stripes for optimally doped Ba(Fe, Co)$_2$As$_2$ ($V = -20$ mV and $I = 0.67$ nA). The trajectories are drawn in the inset of (a). Spectra are offset for clarity. The inset image shows the corresponding topographic image with the size of $25\times50$ Å$^2$. (c) and (d) Intensity plot of the spectra in (a) and (b), respectively.

except that the width of the coherence peaks is very weakly modulated across the stripe [Fig. 5(d)]. This is consistent with the fact that the superconducting coherence length (typically more than 20 Å [7,16]) is much larger than the periodicities of these superlattices.

## IV. SUMMARY

We have performed an STM/STS study on the *AE*-122 iron pnictides. Cleaving at a cryogenic temperature exposes the predominant rt2-buckled *AE* termination and $1\times2$-dimerized As termination. Very occasionally the crystal cleaves between the As and Fe layers leaving the rt2 reconstructed pattern of the Fe layer exposed with characteristic $1\times1$ lattice symmetry. The superconducting energy gap is observed on *AE* and As terminations, while no gap features are found on the Fe termination. Our atomic layer-resolved spectroscopic study suggests that the As-Fe-As trilayer block is essential for the superconductivity in 122 pnictides. The definite identification of various terminating surfaces and detailed spectroscopic characterization on each termination provide us valuable information towards a comprehensive understanding of the iron-based superconductivity. Our methodology of atomic surface identification and layer-revolved tunneling demonstrated here can also be generally applied to study other complex layered quantum materials [37,38].

## ACKNOWLEDGMENTS

We sincerely thank Dr. D. Lu and Dr. Z. Y. Lu for helpful discussions. This work is supported by the Chinese Academy of Sciences, NSFC (11227903), BMSTC (Z181100004218007), the Ministry of Science and Technology of China (2015CB921300, 2015CB921304, 2017YFA0302903), the Strategic Priority Research Program B (XDB04040300, XDB07000000). A.L. acknowledges support from the Shanghai Science and Technology Committee (18ZR1447300). Work at University of Houston was supported by the State of Texas through TcSUH. C.-S.T. acknowledges support of the Robert A. Welch Foundation (E-1146). Work at ORNL was supported by the U. S. Department of Energy, Office of Science, Basic Energy Sciences, Materials Sciences and Engineering Division.

---

[1] Y. Kamihara, T. Watanabe, M. Hirano, and H. Hosono, J. Am. Chem. Soc. **130**, 3296 (2008).

[2] D. Johnston, Adv. Phys. **59**, 803 (2010).

[3] G. R. Stewart, Rev. Mod. Phys. **83**, 1589 (2011).

[4] K. Juroki, S. Onari, R. Arita, H. Usui, Y. Tanaka, H. Kontani, and H. Aoki, New J. Phys. **11**, 025017 (2009).

[5] J. E. Hoffman, Rep. Prog. Phys. **74**, 124513 (2011).

[6] M. C. Boyer, K. Chatterjee, W. D. Wise, G. F. Chen, J. L. Luo, N. L. Wang, and E. W. Hudson, arXiv:0806.4400.

[7] Y. Yin, M. Zech, T. L. Williams, X. F. Wang, G. Wu, X. H. Chen, and J. E. Hoffman, Phys. Rev. Lett. **102**, 097002 (2009).

[8] D. Hsieh, Y. Xia, L. Wray, D. Qian, K. Gomes, A. Yazdani, G. F. Chen, J. L. Luo, N. L. Wang, and M. Z. Hasan, arXiv:0812.2289.

[9] F. Massee, Y. Huang, R. Huisman, S. de Jong, J. B. Goedkoop, and M. S. Golden, Phys. Rev. B **79**, 220517(R) (2009).

[10] V. B. Nascimento, A. Li, D. R. Jayasundara, Y. Xuan, J. O'Neal, S. Pan, T. Y. Chien, B Hu, X. B. He, G. Li, A. S. Sefat, M. A. McGuire, B. C. Sales, D. Mandrus, M. H. Pan, J. Zhang, R. Jin, and E. W. Plummer, Phys. Rev. Lett. **103**, 076104 (2009).

[11] F. C. Niestemski, V. B. Nascimento, B. Hu, W. Plummer, J. Gillett, S. Sebastian, Z. Wang, and V. Madhavan, arXiv:0906.2761.

[12] F. Massee, S. de Jong, Y. Huang, J. Kaas, E. van Heumen, J. B. Goedkoop, and M. S. Golden, Phys. Rev. B **80**, 140507(R) (2009).

[13] T. Chuang, M. Allan, J. Lee, Y. Xie, N. Ni, S. Bud'ko, G. Boebinger, P. Canfield, and J. Davis, Science **327**, 181 (2010).

[14] H. Zhang, J. Dai, Y. Zhang, D. Qu, H. Ji, G. Wu, X. F. Wang, X. H. Chen, B. Wang, C. Zeng, J. Yang, and J. G. Hou, Phys. Rev. B **81**, 104520 (2010).

[15] T. Nishizaki, Y. Nakajima, T. Tamegai, and N. Kobayashi, J. Phys. Soc. Jpn. **80**, 014710 (2011).

[16] L. Shan, Y. Wang, B. Shen, B. Zeng, Y. Huang, A. Li, D. Wang, H. Yang, C. Ren, Q. Wang, S. Pan, and H. Wen, Nat. Phys. **7**, 325 (2011).

[17] M. L. Teague, G. K. Drayna, G. P. Lockhart, P. Cheng, B. Shen, H.-H. Wen, and N.-C. Yeh, Phys. Rev. Lett. **106**, 087004 (2011).

[18] G. Li, X. He, J. Zhang, R. Jin, A. S. Sefat, M. A. McGuire, D. G. Mandrus, B. C. Sales, and E. W. Plummer, Phys. Rev. B **86**, 060512(R) (2012).

[19] K. Koepernik, S. Johnston, E. van Heumen, Y. Huang, J. Kaas, J. B. Goedkoop, M. S. Golden, and J. van den Brink, Phys. Rev. Lett. **109**, 127001 (2012).

[20] Z. Wang, H. Yang, D. Fang, B. Shen, Q. Wang, L. Shan, C. Zhang, P. Dai, and H. Wen, Nat. Phys. **9**, 42 (2013).

[21] I. Zeljkovic, D. Huang, C.-L. Song, B. Lv, C.-W. Chu, and J. E. Hoffman, Phys. Rev. B **87**, 201108(R) (2013).

[22] C.-L. Song, Y. Yin, M. Zech, T. Williams, M. M. Yee, G.-F. Chen, J.-L. Luo, N.-L. Wang, E.W. Hudson, and J. E. Hoffman, Phys. Rev. B **87**, 214519 (2013).

[23] G. Li, L. Liang, Q. Li, M. Pan, V. B. Nascimento, X. He, A. B. Karki, V. Meunier, R. Jin, J. Zhang, and E.W. Plummer, Phys. Rev. Lett. **112**, 077205 (2014).

[24] A. S. Sefat, R. Jin, M. A. McGuire, B. C. Sales, D. J. Singh, and D. Mandrus, Phys. Rev. Lett. **101**, 117004 (2008).

[25] C. Zhang, M. Wang, H. Luo, M. Wang, M. Liu, J. Zhao, D. L. Abernathy, T. A. Maier, K. Marty, M. D. Lumsden, S. Chi, S. Chang, J. A. Rodriguez-Rivera, J. W. Lynn, T. Xiang, J. Hu, and P. Dai, Sci. Rep. **1**, 115 (2011).

[26] B. Lv, L. Deng, M. Gooch, F. Wei, Y. Sun, J. K. Meen, Y. Xue, B. Lorenz, and C.-W. Chu, Proc. Natl. Acad. Sci. USA **108**, 15705 (2011).

[27] S. Ran, S. L. Bud'ko, D. K. Pratt, A. Kreyssig, M. G. Kim, M. J. Kramer, D. H. Ryan, W. N. Rowan-Weetaluktuk, Y. Furukawa, B. Roy, A. I. Goldman, and P. C. Canfield, Phys. Rev. B **83**, 144517 (2011).

[28] M. Rotter, M. Tegel, D. Johrendt, I. Schellenberg, W. Hermes, and R. Pöttgen, Phys. Rev. B **78**, 020503(R) (2008).

[29] N. Ni, M. E. Tillman, J.-Q. Yan, A. Kracher, S. T. Hannahs, S. L. Bud'ko, and P. C. Canfield, Phys. Rev. B **78**, 214515 (2008).

[30] I. Shein and A. Ivanovskii, J. Exp. Theor. Phys. **88**, 107 (2009).

[31] M. Gao, F. Ma, Z.-Y. Lu, and T. Xiang, Phys. Rev. B **81**, 193409 (2010).

[32] J.-X. Yin, Ang Li, X.-X. Wu, Jian Li, Zheng Wu, J.-H. Wang, C.-S. Ting, P.-H. Hor, X. J. Liang, C. L. Zhang, P. C. Dai, X. C. Wang, C. Q. Jin, G. F. Chen, J. P. Hu, Z. -Q. Wang, H. Ding, and S. H. Pan, arXiv:1602.04949.

[33] A. V. Balatsky, I. Vekhter, and J.-X. Zhu, Rev. Mod. Phys. **78**, 373 (2006).

[34] Z. Yin, K. Haule, and G. Kotliar, Nat. Mater. **10**, 932 (2011).

[35] C. Zhang, L. W. Harriger, Z. Yin, W. Lv, M. Wang, G. Tan, Y. Song, D. L. Abernathy, W. Tian, T. Egami, K. Haule, G. Kotliar, and P. Dai, Phys. Rev. Lett. **112**, 217202 (2014).

[36] Y. Huang, R. Pierre, J. Wang, X. Wang, X. Shi, N. Xu, Z. Wu, A. Li, J. Yin, T. Qian, B. Lv, C. Chu, S. Pan, M. Shi, and H. Ding, Chin. Phys. Lett. **30**, 017402 (2013).

[37] J-X. Yin, Zheng Wu, J-H. Wang, Z-Y. Ye, Jing Gong, X-Y. Hou, Lei Shan, Ang Li, X-J. Liang, X-X. Wu, Jian Li, C-S. Ting, Z-Q. Wang, J-P. Hu, P-H. Hor, H. Ding, and S. H. Pan, Nat. Phys. **11**, 543 (2015).

[38] J.-X. Yin, S. S. Zhang, H. Li, K. Jiang, G. Chang, B. Zhang, B. Lian, C. Xiang, I. Belopolski, H. Zheng, T. A. Cochran, S.-Y. Xu, G. Bian, K. Liu, T.-R. Chang, H. Lin, Z.-Y. Lu, Z. Wang, S. Jia, W. Wang, and M. Z. Hasan, Nature (London) **562**, 91 (2018).